International Journal of Fracture **88:** 61–86, 1997.

Cavitation instabilities in plastics and rubber-modified plastics

W.J. CHANG and J. PAN
Mechanical Engineering and Applied Mechanics, The University of Michigan, Ann Arbor, MI 48109

Received 6 June 1997; accepted in revised form to December 1997

Abstract. Spherical void expansion in plastics and rubber-modified plastics is investigated under radial traction conditions. The plastics are modeled as elastic-plastic pressure-sensitive materials and the rubbers are modeled as nonlinearly elastic materials. First, the growth of a spherical void in an infinite plastic matrix is investigated under remote radial traction conditions. The results show that the cavitation stress of the plastic decreases significantly as the pressure sensitivity increases. Then, the growth of a spherical void located at the center of a spherical rubber particle in an infinite plastic matrix is investigated under remote radial traction conditions. The results indicate that without any failure criteria for the rubber, the cavitation stress does not exist when the void is small and the rubber is characterized by high-order strain energy functions. However, when a failure criterion for the rubber is considered at a finite stretch ratio, the results show that the cavitation stress for the plastic with the rubber particle becomes close to that for the plastic without the rubber particle.

Key words: Cavitation instability, cavitation stress, void growth, plastics, rubber, rubber-modified plastics, pressure-sensitive yielding, toughening.

1. Introduction

Nucleation, growth and coalescence of voids are the main physical mechanism in ductile fracture processes of solids. Many studies have been conducted to investigate the influence of microvoid growth on ductile fracture processes. For example, Rice and Tracey (1969) investigated the growth of a spherical void in an infinite Mises material. Gurson (1975) obtained an approximate yield criterion for porous Mises materials by an upper-bound approach. Gurson's yield criterion (1975) and its modified forms (Tvergaard, 1981; Tvergaard, 1982) have been widely used to study ductile fracture processes, for example, see Needleman and Tvergaard (1987) and Tvergaard (1990). Recently, the continuum elastic-plastic theory based on Gurson's yield criterion has been employed to study the effects of void growth and coalescence on crack initiation and growth in ductile solids by Xia and Shih (1995a; 1995b) and Xia, Shih and Hutchinson (1995).

Cavitation instability occurs when the stress level is sufficiently high such that the void expansion rate becomes infinitely large. Examples of material failure due to cavitation can be found in metals (Ashby et al., 1989) and in rubber (Gent and Lindley, 1959). Early work on cavitation instabilities is summarized in Hill (1950). The cavitation problem has been investigated in the context of nonlinear elasticity by Ball (1982). Ball studied a class of bifurcation problems in which a spherical void forms at the center of a sphere of nonlinearly elastic material under surface tractions or displacements. An alternative interpretation for such problems in terms of the growth of a pre-existing microvoid has been given by Horgan and Abeyaratne (1986). An excellent review of cavitation in nonlinearly elastic solids can be found in Horgan and Polignone (1995). For cavitation in elastic-plastic materials, Huang et al. (1991) and Tvergaard et al. (1992) examined cavitation instabilities in Mises materials under both spherically symmetric and axisymmetric conditions. Hou and Abeyaratne (1992)

examined the cavitation in elastic and elastic-plastic solids under non-symmetric loading and presented cavitation criteria in terms of the principal true stresses for neo-Hookean materials and elastic-plastic power-law materials.

Cavitation in rubber particles seems to play an important role in the toughening mechanism of rubber-modified plastics (Yee and Pearson, 1986; Pearson and Yee, 1986, 1991; Yee et al., 1993; Sue and Yee, 1996; Williams and Schapery, 1965; Gent and Wang, 1991; Lazzeri and Bucknall, 1993; Jeong and Pan, 1996). Therefore, a thorough understanding of the cavitation behavior in rubber-modified plastics is essential to understand the toughening. The theoretical framework of Ball (1982) and Horgan and Abeyaratne (1986) have provided insight into cavitation in nonlinearly elastic materials. However, there are still some inconsistencies that need to be explored. For example, the critical surface tractions for neo-Hookean materials obtained from the bifurcation approach agree with those observed in the internal rupture of rubber in Gent and Lindley (1959). However, the critical traction becomes unbounded for Mooney-Rivlin materials or nonlinearly elastic materials characterized by higher-order strain energy functions (Horgan and Polignone, 1995). Chang and Pan (1998) investigated this inconsistency by considering a simple strain failure criterion for rubber at large strains. They found that cavitation instability can be consistently predicted in rubbers characterized by different strain energy functions with consideration of rubber failure at large strains.

In this paper, we explore the implications of a failure criterion for rubber at large strains on cavitation instability in rubber-modified plastics in a spirit consistent with those of Ball (1982) and Horgan and Polignone (1995) for nonlinearly elastic materials. First, we examine the growth of a spherical void in an infinite plastic matrix subjected to remote radial traction conditions. Then, we examine the growth of a spherical void at the center of a spherical rubber particle in an infinite plastic matrix subjected to remote radial traction conditions with and without consideration of rubber failure. Finally, the results for the plastic and for the rubber-modified plastic are compared and discussed.

2. Spherical void expansion in plastics

In this section, spherical void expansion in an infinite plastic matrix under remote radial traction is investigated. The undeformed and deformed configurations for a spherical void in a plastic matrix are schematically shown in Figure 1. As shown in Figure 1(a) for the undeformed configuration, the center of the spherical void with the initial radius r_0 is located at the origin of a spherical coordinate (r, θ, ϕ) system. As shown in Figure 1(b) for the deformed configuration, the remote radial stress σ_∞ is applied at the infinity and the radius of the void becomes R_0 after σ_∞ is applied. We assume that a material point initially located at r measured from the center of the void moves to R in the deformed configuration after σ_∞ is applied. Here, the rigid body motion is not considered. Also, we denote the radius of the plastic zone as C in the deformed configuration so that the material inside the boundary $R = C$ is plastically deformed and the material outside the boundary $R = C$ remains elastic under the remote radial stress σ_∞.

The relation between the radial stress σ_∞ and the void expansion ratio R_0/r_0 for materials with different values of pressure sensitivity, with or without strain hardening, are investigated here. When the remote radial stress approaches to a critical cavitation stress of the material, the void expansion ratio becomes infinitely large. In general, engineering materials contain pre-existing microvoids. Therefore these initially invisible microvoids can become very large when the critical cavitation stress is reached.

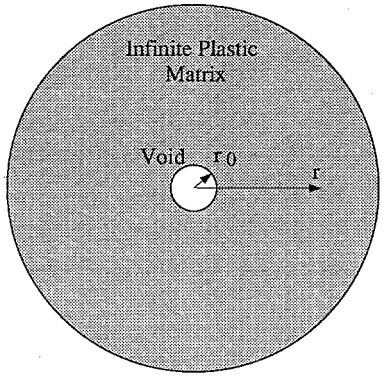

(a) Undeformed Configuration

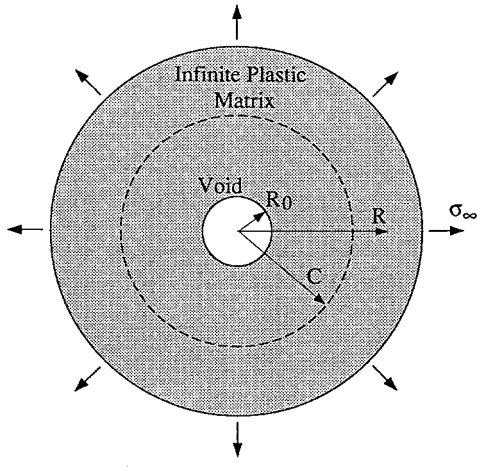

(b) Deformed Configuration

Figure 1. A spherical void in an infinite plastic matrix. (a) undeformed configuration, (b) deformed configuration.

2.1. CONSTITUTIVE MODELING OF PLASTICS

The Drucker–Prager yield criterion (Drucker, 1973; Drucker and Prager, 1952; Li and Pan, 1990a; Li and Pan, 1990b), which is a linear combination of the effective stress σ_e and the mean stress σ_m, is adopted here to model the yielding in the plastic matrix

$$\psi(\sigma_{ij}) = \sigma_e + \sqrt{3}\mu\sigma_m = \sigma_{ge}, \tag{1}$$

where $\sigma_e = (3s_{ij}s_{ij}/2)^{1/2}$, $s_{ij} = \sigma_{ij} - \sigma_m\delta_{ij}$, and $\sigma_m = \sigma_{kk}/3$. Here, δ_{ij} is the Kronecker delta and the subscripts i, j and k have the range of 1 to 3. In (1), $\psi(\sigma_{ij})$ represents the yield surface in the stress space and μ represents the pressure sensitivity of the plastic. Here σ_{ge} is the generalized tensile effective stress and represents the size of the yield surface in the stress space.

In this study, μ is assumed to be a material constant and can be determined from the initial uniaxial compressive yield stress σ_c and the initial uniaxial tensile yield stress σ_t as

$$\mu = \sqrt{3}\frac{\sigma_c - \sigma_t}{\sigma_c + \sigma_t}. \tag{2}$$

The initial yield surface can be specified by $\sigma_{ge} = \sigma_0$, where σ_0 is the initial generalized tensile effective stress and can be determined by

$$\sigma_0 = \frac{2\sigma_c\sigma_t}{\sigma_c + \sigma_t}. \tag{3}$$

For perfectly plastic materials, the generalized effective stresses σ_{ge} becomes a constant represented by σ_0 when yielding occurs.

A plastic potential function ϕ_p is defined as

$$\phi_p(\sigma_{ij}) = \sigma_e + \sqrt{3}\beta\sigma_m = \sigma_\alpha, \tag{4}$$

where β is the plastic dilatancy factor and σ_α represents the size of the plastic potential surface. For normality plastic flow, $\beta = \mu$. For incompressible plastic flow, $\beta = 0$. The plastic part of the strain rate tensor, $\dot{\epsilon}^p_{ij}$, can be derived from the plastic potential ϕ_p as

$$\dot{\epsilon}^p_{ij} = \dot{\lambda}\frac{\partial\phi_p}{\partial\sigma_{ij}} = \dot{\lambda}\left(\frac{3s_{ij}}{2\sigma_e} + \frac{\beta}{\sqrt{3}}\delta_{ij}\right), \tag{5}$$

where $\dot{\lambda}$ represents a proportionality factor.

The proportionality factor $\dot{\lambda}$ in (5) can be determined from the equivalence of plastic work rate

$$\dot{W}^p = \sigma_{ij}\dot{\epsilon}^p_{ij} = \sigma_{ge}\dot{\epsilon}^p_{ge}, \tag{6}$$

where $\dot{\epsilon}^p_{ge}$ is the generalized equivalent plastic strain rate. Substituting (5) into (6) gives

$$\dot{\lambda} = \frac{\sigma_{ge}}{\sigma_\alpha}\dot{\varepsilon}^p_{ge}, \tag{7}$$

where σ_α is defined in (4). Therefore, (5) becomes

$$\dot{\epsilon}^p_{ij} = \dot{\epsilon}^p_{ge}\frac{\sigma_{ge}}{\sigma_\alpha}\left(\frac{3s_{ij}}{2\sigma_e} + \frac{\beta}{\sqrt{3}}\delta_{ij}\right). \tag{8}$$

The relation between the stresses and the plastic strains for the corresponding deformation plasticity theory is

$$\epsilon^p_{ij} = \epsilon^p_{ge}\frac{\sigma_{ge}}{\sigma_\alpha}\left(\frac{3s_{ij}}{2\sigma_e} + \frac{\beta}{\sqrt{3}}\delta_{ij}\right). \tag{9}$$

Based on Hooke's law for isotropic linear elastic materials, the elastic part of the strain can be represented as

$$\epsilon^e_{ij} = \frac{1}{E}[(1+\nu)\sigma_{ij} - \nu\sigma_{kk}\delta_{ij}]. \tag{10}$$

Therefore, the total strain ϵ_{ij} can be expressed as

$$\epsilon_{ij} = \epsilon_{ij}^e + \epsilon_{ij}^p = \frac{1}{E}[(1+\nu)\sigma_{ij} - \nu\sigma_{kk}\delta_{ij}] + \epsilon_{ge}^p \frac{\sigma_{ge}}{\sigma_\alpha}\left(\frac{3s_{ij}}{2\sigma_e} + \frac{\beta}{\sqrt{3}}\delta_{ij}\right). \tag{11}$$

A relation between σ_{ge} and ϵ_{ge}^p for power-law hardening materials is assumed as

$$\epsilon_{ge}^p/\epsilon_0 = \begin{cases} 0 & \text{if } \sigma_{ge} < \sigma_0 \\ (\sigma_{ge}/\sigma_0)^n - 1 & \text{if } \sigma_{ge} \geqslant \sigma_0, \end{cases} \tag{12}$$

where σ_0 is the initial generalized tensile effective stress, n is the hardening exponent, ϵ_0 is defined by $\epsilon_0 \equiv \sigma_0/E$, and E is Young's modulus.

It is well known that deformation plasticity theory is inadequate where there is a large departure from proportional loading conditions. However, when the loading is nearly proportional, the deformation plasticity theory can be considered no more objectionable than the corresponding incremental flow theory (Budiansky, 1959). In fact, Huang et al. (1991) obtained almost the same numerical results for the critical cavitation stresses in perfectly plastic Mises materials based on a deformation plasticity theory and the corresponding incremental plasticity theory. In this study, we only adopt the deformation plasticity stress-strain relation specified in (11) for the plastic.

2.2. Formulation for hardening materials

Recall the initial void radius is r_0 and the void radius becomes R_0 after the remote radial stress σ_∞ is applied. The governing equations for the stresses, strains, and displacement are formulated based on the deformed configuration. We assume that the outer region remains elastic and the remote radial stress is high enough so that a plastic region develops from the surface of the void based on the deformed configuration. Assume that the elastic-plastic boundary is at $R = C$, where $C \geqslant R_0$. Due to symmetry, the non-vanishing stresses are σ_R, σ_θ, and $\sigma_\phi (= \sigma_\theta)$. The non-vanishing strains are $\epsilon_R, \epsilon_\theta$, and $\epsilon_\phi (= \epsilon_\theta)$. The only non-vanishing displacement is u_R. Note that the rigid body motion of the material is not considered.

We begin by considering the stresses and displacement in the outer elastic region. The small-strain theory is used to obtain closed-form solutions for the outer elastic field to avoid integration from the infinity. The radial stress σ_R in the outer elastic region has the form (1951).

$$\sigma_R = \frac{A_1}{R^3} + A_2, \tag{13}$$

where A_1 and A_2 are the constants to be determined from the boundary conditions at $R = \infty$ and $R = C$.

The equilibrium equation for the spherically symmetric problem is

$$\frac{\mathrm{d}\sigma_R}{\mathrm{d}R} + \frac{2}{R}(\sigma_R - \sigma_\theta) = 0. \tag{14}$$

Substituting (13) into (14) and solving the resulting differential equation with the two boundary conditions $\sigma_R(R \to \infty) = \sigma_\infty$ and $\sigma_{ge}(R = C) = \sigma_0$ give the stresses in the outer elastic region as

$$\sigma_R = \sigma_\infty - \tfrac{2}{3}(\sigma_0 - \sqrt{3}\mu\sigma_\infty)\frac{C^3}{R^3} \tag{15}$$

$$\sigma_\theta = \sigma_\infty + \tfrac{1}{3}(\sigma_0 - \sqrt{3}\mu\sigma_\infty)\frac{C^3}{R^3}. \tag{16}$$

Then, (15) and (16) are substituted into (10) to solve for the strains in the outer elastic region.

From the small-strain theory, we have

$$\epsilon_R = \frac{\mathrm{d}u_R}{\mathrm{d}R} \tag{17}$$

$$\epsilon_\theta = \frac{u_R}{R}. \tag{18}$$

The displacement u_R in the outer elastic region can be obtained as

$$u_R = \left[(1-2\nu)\frac{\sigma_\infty}{E}\right] R + \frac{(1+\nu)}{3}\left[\frac{\sigma_0 - \sqrt{3}\mu\sigma_\infty}{E}\right]\frac{C^3}{R^2}. \tag{19}$$

Note that we use the small-strain theory to obtain the outer boundary conditions for the inner plastic region to simplify our problem because the deformation in the elastic region is quite small and the small-strain theory should be adequate.

The values of the stresses and displacement at the elastic-plastic boundary $R = C$ will be used for starting numerical integration for the stresses and displacement in the inner plastic region where the finite deformation effects must be considered. From (15), (16), and (19), the non-vanishing stresses and displacement at $R = C$ are

$$\sigma_R^C = \left(1 + \frac{2}{\sqrt{3}}\mu\right)\sigma_\infty - \tfrac{2}{3}\sigma_0 \tag{20}$$

$$\sigma_\theta^C = \left(1 - \frac{1}{\sqrt{3}}\mu\right)\sigma_\infty + \tfrac{1}{3}\sigma_0 \tag{21}$$

$$u_R^C = \frac{C}{E}\left\{\frac{1+\nu}{3}\sigma_0 + \left[1 - 2\nu - \frac{(1+\nu)\mu}{\sqrt{3}}\right]\sigma_\infty\right\}. \tag{22}$$

Note that the radius of the inner plastic region, C, is not yet determined.

In order to solve the stresses, strains and displacement in the inner plastic region, (11) is first written as

$$\epsilon_R = \frac{1}{E}[\sigma_R - 2\nu\sigma_\theta] + \epsilon_{ge}^p\left(\frac{\sigma_{ge}}{\sigma_\alpha}\right)\left(-1 + \frac{\beta}{\sqrt{3}}\right) \tag{23}$$

$$\epsilon_\theta = \frac{1}{E}[-\nu\sigma_R + (1-\nu)\sigma_\theta] + \epsilon_{ge}^p\left(\frac{\sigma_{ge}}{\sigma_\alpha}\right)\left(\frac{1}{2} + \frac{\beta}{\sqrt{3}}\right), \tag{24}$$

where ϵ_{ge}^p is expressed as

$$\frac{\epsilon_{ge}^p}{\epsilon_0} = (\sigma_{ge}/\sigma_0)^n - 1 \tag{25}$$

as in (12). For the spherically symmetric problem, we have

$$\sigma_{ge} = \sigma_\theta - \sigma_R + \frac{\mu}{\sqrt{3}}(\sigma_R + 2\sigma_\theta) \tag{26}$$

$$\sigma_\alpha = \sigma_\theta - \sigma_R + \frac{\beta}{\sqrt{3}}(\sigma_R + 2\sigma_\theta) \tag{27}$$

by assuming $\sigma_\theta \geqslant \sigma_R$.

When finite deformation is considered, the strains are defined as

$$\epsilon_R = \ln\left\{\frac{\mathrm{d}R}{\mathrm{d}R - \mathrm{d}u_R}\right\} = -\ln(1 - \mathrm{d}u_R/\mathrm{d}R) \tag{28}$$

$$\epsilon_\theta = \ln\left\{\frac{R}{R - u_R}\right\} = -\ln(1 - u_R/R), \tag{29}$$

where we recall that $u_R = R - r$. Substituting (28) into (23) and then (29) into (24) gives

$$\frac{\mathrm{d}u_R}{\mathrm{d}R} = 1 - \exp\left[-\frac{\sigma_R - 2\nu\sigma_\theta}{E} - \epsilon_{ge}\left(\frac{\sigma_{ge}}{\sigma_\alpha}\right)\left(-1 + \frac{\beta}{\sqrt{3}}\right)\right] \tag{30}$$

$$\frac{u_R}{R} = 1 - \exp\left[\frac{-(1-\nu)\sigma_\theta - \nu\sigma_R}{E} - \epsilon_{ge}\left(\frac{\sigma_{ge}}{\sigma_\alpha}\right)\left(\frac{1}{2} + \frac{\beta}{\sqrt{3}}\right)\right]. \tag{31}$$

Also, the equilibrium equation (14) can be written as

$$\frac{\mathrm{d}\sigma_R}{\mathrm{d}R} = \frac{2}{R}(\sigma_\theta - \sigma_R). \tag{32}$$

The governing equations of the inner plastic region for power-law hardening materials are now reduced to (30), (31), and (32).

Note that σ_R, σ_θ, and u_R are all functions of R. Therefore, (30) and (32) can be used to integrate for σ_R and u_R and (31) gives a nonlinear equation for σ_θ, which has to be solved by numerical iterations. Note that we use the small-strain theory to define the strains in the elastic region whereas we use the logarithmic strain definition to define the strains in the plastic region. At $R = C$, we use the stresses, strains, and displacement from the elastic region based on the small-strain theory as the boundary conditions to start the integration of (30) to (32) which are based on the logarithmic strains. However, the strains at $R = C$ are quite small and the elastic solutions based on the small-strain theory should be good approximations.

The numerical procedures to solve the stresses and displacement in the inner plastic region are given in the following. Note that the stresses σ_R and σ_θ, and the displacement u_R are referring to the current deformed configuration. The size of the inner plastic region, C, is first given as an initial guess. Based on the initial guess value of C, σ_R, σ_θ, and u_R at $R = C$ are obtained from (20), (21), and (22). From the continuity conditions of σ_R and u_R at $R = C$, the values of σ_R and u_R at $R = C$ are used to initiate numerical integration for σ_R, σ_θ, and u_R in the inner plastic region. A combined fourth-fifth order Runge–Kutta scheme with error and step-size control is employed to solve (30), (31) and (32) from $R = C$ to $R = R_0$.

At each step of the integration, the values of $\mathrm{d}\sigma_R/\mathrm{d}R$ and $\mathrm{d}u_R/\mathrm{d}R$ are calculated from (32) and (30) respectively, and (31) is used to obtain σ_θ by numerical iterations. The numerical

integration is performed until the surface of the void ($R = R_0$) is reached. On the surface of the void, the traction-free boundary condition requires

$$\sigma_R = 0 \quad \text{at} \quad R = R_0. \tag{33}$$

If the boundary condition in (33) is not satisfied, a new value of C is assigned. Numerical iterations are performed to find the value of C to satisfy (33). After C is found, these σ_R, σ_θ and u_R as functions of R are the solutions for the inner plastic region. Then, the expansion ratio of the void is calculated from

$$R_0/r_0 = R_0/(R_0 - u_R(R = R_0)). \tag{34}$$

The numerical iterations to find C to satisfy (33) and to find σ_θ to satisfy (31) require good initial guesses to reach convergent results. Therefore, the remote radial stress σ_∞ is increased incrementally from the value at which yielding starts to develop on the surface of the void at $R = R_0$. This value of σ_∞ can be determined by solving (20) with $\sigma_R^C = 0$ and the result is $\sigma_\infty = 2\sigma_0/(3 + 2\sqrt{3}\mu)$. As the remote radial stress σ_∞ increases, the radius of the plastic zone C increases. The solution of C for the current value of σ_∞ is used as the initial guess of C for a larger value of σ_∞. In the same manner, when σ_R, σ_θ and u_R are integrated from $R = C$ to $R = R_0$, the initial guess of σ_θ for solving σ_θ by (31) at each integration step is taken from the last integration step.

2.3. Formulation for perfectly plastic materials

For elastic perfectly plastic materials, the solution procedure is quite similar to that for elastic power-law hardening materials. However, for elastic perfectly plastic materials, the governing equations can be reduced to simpler forms and the stresses can be solved independently from the strains and displacement. In some special cases, closed-form solutions for the relation between the normalized remote radial stress σ_∞/σ_0 and the void expansion ratio R_0/r_0 can be obtained. These closed-form solutions are especially useful for validating our numerical solutions.

The solutions for the outer elastic region are the same as those for hardening materials. Also, the stresses in the inner plastic region for perfectly plastic materials can be solved with the use of the equilibrium equation (14) and the yield condition

$$\sigma_{ge} = (\sigma_\theta - \sigma_R) + \sqrt{3}\mu \left[\frac{\sigma_R + 2\sigma_\theta}{3}\right] = \sigma_0, \tag{35}$$

where we have implicitly assumed that $\sigma_\theta \geqslant \sigma_R$. Substituting (35) into (14) and applying the traction boundary condition $\sigma_R = 0$ at $R = R_0$ give the stresses in the inner plastic region as

$$\sigma_R = \frac{\sigma_0}{\sqrt{3}\mu}\left[1 - \left(\frac{R}{R_0}\right)^{-6\mu/(\sqrt{3}+2\mu)}\right] \tag{36}$$

$$\sigma_\theta = \frac{\sqrt{3}\sigma_0}{\sqrt{3} + 2\mu}\left\{1 + \frac{\sqrt{3} - \mu}{3\mu}\left[1 - \left(\frac{R}{R_0}\right)^{-6\mu/(\sqrt{3}+2\mu)}\right]\right\}, \tag{37}$$

where $\mu > 0$. From (36) and (20) and the continuity condition of σ_R at $R = C$, the closed-form solution of C is given as

$$\frac{C}{R_0} = \left[\left(1 + \frac{2\mu}{\sqrt{3}}\right)\left(1 - \sqrt{3}\mu\frac{\sigma_\infty}{\sigma_0}\right)\right]^{-\frac{\sqrt{3}+2\mu}{6\mu}}. \tag{38}$$

In order to solve the strains and displacement in the inner plastic region, (11) is written as

$$\epsilon_R = \frac{1}{E}[\sigma_R - 2\nu\sigma_\theta] + \epsilon^p_{ge}\frac{\sigma_{ge}}{\sigma_\alpha}\left(-1 + \frac{\beta}{\sqrt{3}}\right) \tag{39}$$

$$\epsilon_\theta = \frac{1}{E}[-\nu\sigma_R + (1-\nu)\sigma_\theta] + \epsilon^p_{ge}\frac{\sigma_{ge}}{\sigma_\alpha}\left(\frac{1}{2} + \frac{\beta}{\sqrt{3}}\right). \tag{40}$$

Let $\beta_1 = -1 + \beta/\sqrt{3}$ and $\beta_2 = 1/2 + \beta/\sqrt{3}$. Multiplying (39) by β_2 and (40) by $-\beta_1$ and adding the results together, we have

$$\beta_2\epsilon_R - \beta_1\epsilon_\theta = F(R), \tag{41}$$

where

$$F(R) = \frac{1}{E}[(\beta_2 + \nu\beta_1)\sigma_R + ((\beta_1 - 2\beta_2)\nu - \beta_1)\sigma_\theta]. \tag{42}$$

Here, the solutions for the stresses σ_R and σ_θ are expressed in (36) and (37).

Substituting (28) and (29) into (41) results in

$$\ln\frac{(1 - u_R/R)^{\beta_1}}{(1 - \mathrm{d}u_R/\mathrm{d}R)^{\beta_2}} = F(R). \tag{43}$$

Equation (43) can be rewritten as

$$\frac{\mathrm{d}u_R}{\mathrm{d}R} = 1 - (1 - u_R/R)^{\beta_1/\beta_2}\exp[-F(R)/\beta_2]. \tag{44}$$

Equation (44) and the boundary condition of u_R at $R = C$, (22), are then used to integrate u_R from $R = C$ to $R = R_0$ by the Runge–Kutta integration scheme. After $u_R(R = R_0)$ is obtained, the void expansion ratio is calculated by (34).

For Mises materials ($\mu = \beta = 0$), (38), (36), and (37) become invalid. For Mises materials, the yield condition gives

$$\sigma_{ge} = \sigma_\theta - \sigma_R = \sigma_0. \tag{45}$$

Substituting (45) into (14) and applying the boundary condition $\sigma_R(R = R_0) = 0$ result in the closed-form solutions of σ_R and σ_θ as

$$\sigma_R = 2\sigma_0 \ln\left(\frac{R}{R_0}\right) \tag{46}$$

$$\sigma_\theta = \sigma_0 + 2\sigma_0 \ln\left(\frac{R}{R_0}\right). \tag{47}$$

From the continuity condition of σ_R at $R = C$, (46) and (20) lead to

$$\frac{C}{R_0} = \exp\left(\frac{1}{2}\frac{\sigma_\infty}{\sigma_0} - \frac{1}{3}\right). \tag{48}$$

Substituting (48) into (22) gives

$$u_R(R = C) = R_0\epsilon_0\left\{(1-2\nu)\frac{\sigma_\infty}{\sigma_0} + \frac{1+\nu}{3}\right\}\exp\left(\frac{1}{2}\frac{\sigma_\infty}{\sigma_0} - \frac{1}{3}\right) \tag{49}$$

The analysis of the displacement field for pressure-sensitive materials is also valid for Mises materials. For Mises materials, the governing equation of u_R, (44), becomes

$$\frac{\mathrm{d}u_R}{\mathrm{d}R} = 1 - \left(1 - \frac{u_R}{R}\right)^{-2}\exp\{-2F(R)\}. \tag{50}$$

With the use of (46), (47), and (41), the function $F(R)$ in (50) becomes

$$F(R) = \frac{(1-2\nu)\sigma_0}{E}\left\{1 + 3\ln\left(\frac{R}{R_0}\right)\right\}. \tag{51}$$

Closed-form solutions for the relation between the normalized radial stress σ_∞/σ_0 and the void expansion ratio R_0/r_0 for incompressible materials are presented in the Appendix. These closed-form solutions can be used to validate our numerical solutions. For Mises materials ($\mu = \beta = 0$) with $\nu = 1/2$, the closed-form solution for the relation between the normalized remote radial stress σ_∞/σ_0 and the void expansion ratio R_0/r_0 is presented in (A7) and the critical cavitation stress S/σ_0 is presented in (A8). For pressure-sensitive incompressible materials, the solutions for the relation between σ_∞/σ_0 and R_0/r_0 and the critical cavitation stress S/σ_0 are obtained in (A10) and (A11), respectively. Equation (A13) gives an approximate solution of the critical cavitation stress for pressure-sensitive incompressible materials with reasonable accuracy.

2.4. Numerical results

The void expansion ratios R_0/r_0 at different values of the remote radial stress σ_∞/σ_0 are calculated for both power-law hardening materials and perfectly plastic materials. The relation between σ_∞/σ_0 and R_0/r_0 also depends on the material properties $\mu, \beta, \epsilon_0, \nu$, and n.

In our numerical calculations, the void expansion ratio R_0/r_0 larger than 10^4 can be obtained by gradually increasing the value of σ_∞/σ_0. Therefore, the critical cavitation stress, S/σ_0, is taken as the value of the normalized remote radial stress σ_∞/σ_0 corresponding to $R_0/r_0 = 10^4$ in our numerical calculations. In some special cases for perfectly plastic materials where closed-form solutions of the relation between σ_∞/σ_0 and R_0/r_0 are available, the critical cavitation stress S/σ_0 is defined as the remote radial stress when R_0/r_0 approaches to ∞. Note that in reality, the void expansion ratio must be finite. Cracks or other failure mechanisms develop near the void surface and, consequently, the load-carrying capacity of the surface material elements decreases. Further discussions on the loss of load-carrying capacity of the surface material elements will be given later.

The critical cavitation stresses for materials with $\beta = \mu, \nu = 1/2$, and different values of μ's, n's, and σ_0/E's are listed in Table 1. In general, S/σ_0 decreases as σ_0/E increases and/or

Table 1. The critical cavitation stresses S/σ_0 for pressure-sensitive materials with $\beta = \mu$ and $\nu = 0.5$. The symbol '–' indicates that the critical cavitation stress does not occur when the outer field is elastic.

	σ_0/E	$\mu = 0$	$\mu = 0.1$	$\mu = 0.2$	$\mu = 0.3$
	0.001	5.00	3.59	2.57	1.88
$n = \infty$	0.003	4.27	3.25	2.44	1.85
	0.025	2.86	2.45	2.05	1.70
	0.001	5.15	3.67	2.61	1.90
$n = 100$	0.003	4.37	3.32	2.48	1.87
	0.025	2.91	2.48	2.08	1.71
	0.001	6.85	–	–	–
$n = 10$	0.003	5.52	4.03	2.83	–
	0.025	3.32	2.80	2.30	1.84

Table 2. The critical cavitation stresses S/σ_0 for power-law hardening materials with $n = 10, \sigma_0/E = 0.025$, and $\nu = 0.5$ for different combinations of μ and β

	$\mu = 0$	$\mu = 0.1$	$\mu = 0.2$	$\mu = 0.3$
$\beta = 0$	3.32	2.57	2.02	1.61
$\beta = \mu/2$	3.32	2.69	2.16	1.74
$\beta = \mu$	3.32	2.80	2.30	1.84

μ increases. The normalized critical cavitation stresses S/σ_0 for Mises materials with $n = \infty$ (perfectly plastic materials) and 10 and $\sigma_0/E = 0.001$ and 0.003 are the same as those in Huang et al. (1991) to the accuracy of two decimal digits. Also, the critical cavitation stresses for low-hardening materials with $n = 100$ are found within 3 percent of the corresponding solutions for perfectly plastic materials. In Table 1 for $n = 10$, the symbol '$-$' indicates that infinite void expansion ratio does not occur when the remote region is elastic. Since these conditions occur at very small values of σ_0/E and the value of σ_0/E is usually larger than 0.01 for plastics, void expansion with no remote elastic region is not considered here.

The relations between the void expansion ratio R_0/r_0 and the normalized remote radial stress σ_∞/σ_0 are plotted in Figure 2 for materials with $\epsilon_0 = \sigma_0/E = 0.025$, $n = 10, \nu = 0.5$. We consider three plastic dilatancy factors, $\beta = \mu, \beta = \mu/2$, and $\beta = 0$ for each μ and we take $\mu = 0, 0.1, 0.2$, and 0.3. As shown in the figure, in general, as the normalized remote radial stress becomes larger than 1, the void expansion rate increases. As μ increases, the normalized radial stress σ_∞/σ_0 at a given large R_0/r_0 decreases. For a given μ, the normalized radial stress σ_∞/σ_0 at a given large R_0/r_0 decreases as β decreases. The corresponding critical cavitation stresses for these curves in Figure 2 are listed in Table 2. The pressure sensitivity μ has significant effects on reducing the critical cavitation stress. For example, the critical cavitation stress S/σ_0 for $\mu = \beta = 0$ is 3.32 and the value of S/σ_0 decrease to 1.61 for $\mu = 0.3$ and $\beta = 0$. It should be noted that the value of the critical cavitation stress S/σ_0 is

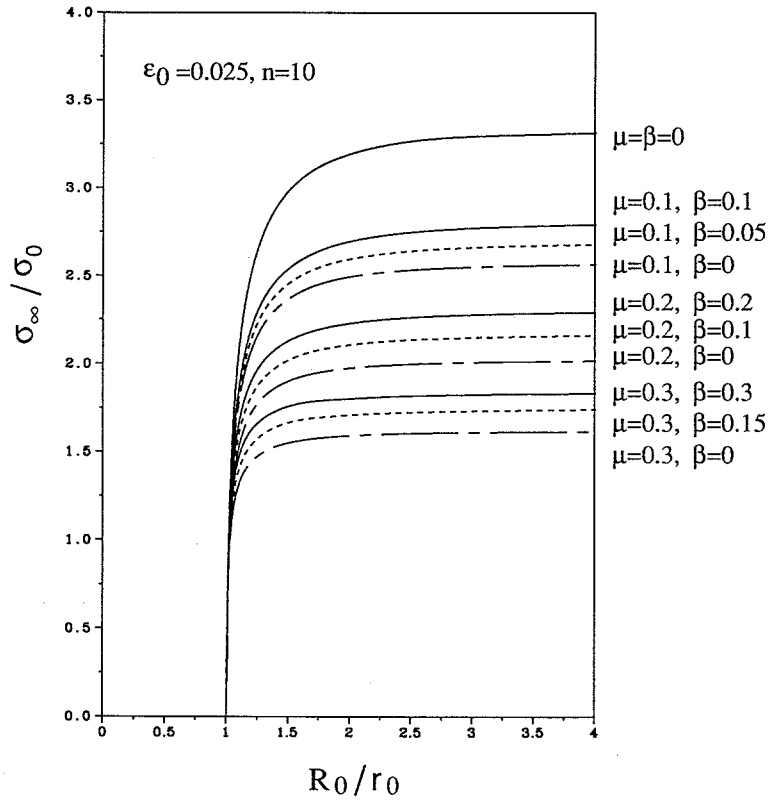

Figure 2. The normalized remote radial stresses σ_∞/σ_0 as functions of the void expansion ratio R_0/r_0 for power-law hardening materials with $\sigma_0/E = 0.025$ and $n = 10$. Results are shown for different values of μ's ($= 0, 0.1, 0.2$ and 0.3) and β's ($= \mu, \mu/2$ and 0).

as low as 1.61 for the case with $\mu = 0.3$ and $\beta = 0$ when compared with typical values of 4 to 5 for metals.

Note that we can represent σ_0 in terms of μ and σ_t as

$$\sigma_0 = \left(1 + \frac{\mu}{\sqrt{3}}\right)\sigma_t. \tag{52}$$

Here, σ_t represents the yield stress in tension. Equation (52) is derived from (2) and (3). When the tensile yield stress σ_t is taken as a given material constant from a tensile test, (52) indicates that the value of σ_0 increases as μ increases. For example, the value of σ_0 for $\mu = 0.3$ is 117.3 percent of the value of σ_0 for $\mu = 0$. Therefore, for $\beta = 0$, the critical cavitation stress S for $\mu = 0.3$ is 57 percent of the value of S for $\mu = 0$. The predictions of the critical cavitation stresses S can differ by a factor of 1.75 with and without considering the effect of pressure sensitivity for a material with $\mu = 0.3$ and $\beta = 0$ using the tensile yield stress σ_t as the input.

Figure 3 shows the relations between R_0/r_0 and σ_∞/σ_0 for perfectly plastic materials with $\epsilon_0 = \sigma_0/E = 0.025$ and $\nu = 0.5$, obtained by the Runge–Kutta numerical integration scheme. The general trends shown in Figure 3 for perfectly plastic materials are quite similar to those shown in Figure 2 for power-law hardening materials. The critical cavitation stresses S/σ_0 for the curves in Figure 3 are listed in Table 3. The approximate closed-form solution of the critical cavitation stress S/σ_0 for perfectly plastic pressure-sensitive incompressible

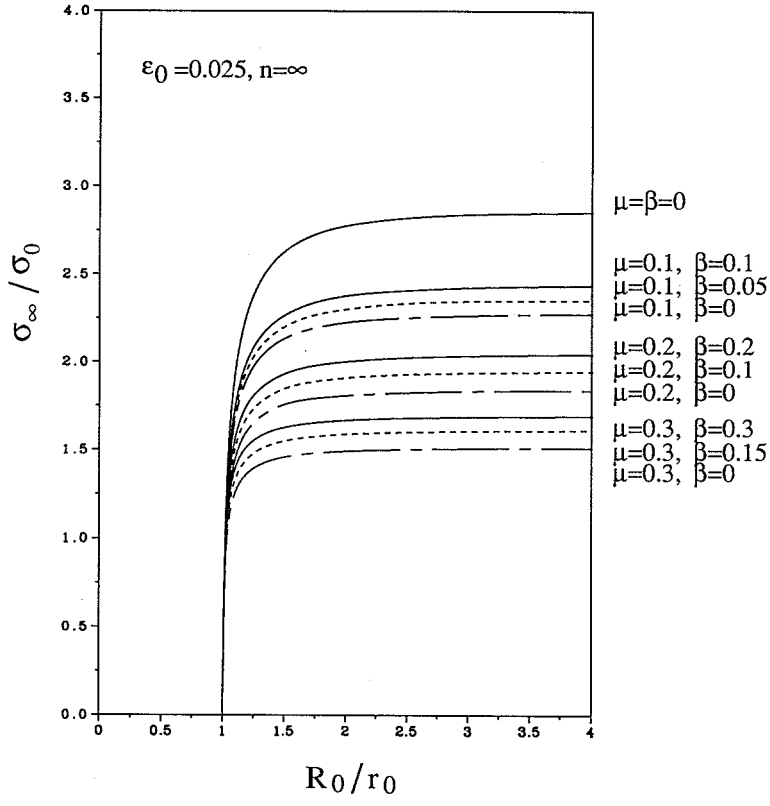

Figure 3. The normalized remote radial stresses σ_∞/σ_0 as functions of the void expansion ratio R_0/r_0 for perfectly plastic materials $(n = \infty)$ with $\sigma_0/E = 0.025$. Results are shown for different values of μ's $(= 0, 0.1, 0.2$ and $0.3)$ and β's $(= \mu, \mu/2$, and $0)$.

Table 3. The critical cavitation stresses S/σ_0 for perfectly plastic materials with $\sigma_0/E = 0.025$ and $\nu = 0.5$ for different combinations of μ and β

	$\mu = 0$	$\mu = 0.1$	$\mu = 0.2$	$\mu = 0.3$
$\beta = 0$	2.86	2.28	1.84	1.51
$\beta = \mu/2$	2.86	2.36	1.95	1.61
$\beta = \mu$	2.86	2.45	2.05	1.70

materials can be obtained from (A13) in Appendix A. The approximate critical cavitation stresses obtained from (A13) for $\epsilon_0 = \sigma_0/E = 0.025$ with $\mu = 0.0001, 0.1, 0.2$, and 0.3 are 2.85, 2.28, 1.84, and 1.51, respectively. These solutions agree very well with the corresponding critical cavitation stresses for $\beta = 0$ obtained from the Runge–Kutta numerical integration scheme listed in Table 3.

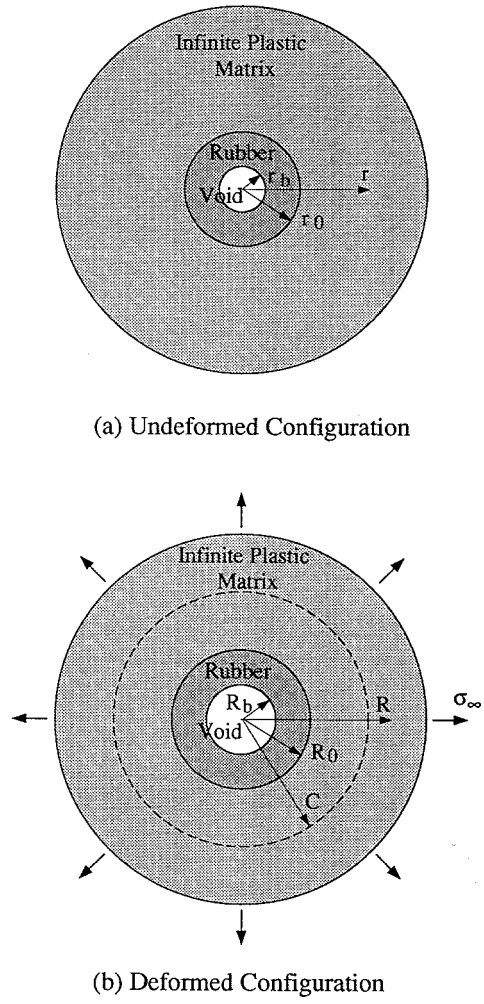

Figure 4. A void in a spherical rubber particle embedded in an infinite plastic matrix. (a) undeformed configuration, (b) deformed configuration.

3. Spherical void expansion in rubber-modified plastics

Spherical void expansion in rubber-modified plastics is investigated in this section. As schematically shown in Figure 4(a), a rubber particle with an initial radius r_0 is embedded in an infinite plastic matrix. A small void with the initial radius r_b is located at the center of the rubber particle. As schematically shown in Figure 4(b), the radius of the void becomes R_b, the radius of the rubber particle becomes R_0, and the size of the plastic region grows to C after the remote radial stress σ_∞ is applied. The rigid body motion is not considered. As the remote radial stress σ_∞ increases, the void in the rubber particle expands. Therefore, R_b, R_0, and C increase as σ_∞ increases. Here, we compare the increase of the radius of the rubber particle in the rubber-modified plastic and the void expansion in the plastic with the initial size of the rubber particle in the voided rubber-modified plastic equal to the initial size of the void in the voided plastic to investigate the effects of the addition of rubber particles on the cavitation stresses of rubber-modified plastics. For the completeness of presentation, we here

summarize the constitutive relations and governing equations for the analysis of cavitation in several rubbers presented in Chang and Pan (1998).

3.1. Constitutive modeling of rubbers

As in Chang and Pan (1998), we adopt a third-order strain energy function investigated by James, Green and Simpson (1975) and James and Green (1975)

$$W = C_{10}(I_1-3) + C_{01}(I_2-3) + C_{11}(I_1-3)(I_2-3) + C_{20}(I_1-3)^2 + C_{30}(I_1-3)^3, \tag{53}$$

where I_1 and I_2 are the first and second invariants of the left Cauchy–Green strain tensor B_{ij}. Note that (53) reduces to the strain energy function for Mooney–Rivlin materials when $C_{11} = C_{20} = C_{30} = 0$ and reduces to that for neo-Hookean materials when $C_{01} = C_{11} = C_{20} = C_{30} = 0$. The components of the Cauchy stress, σ_{ij}, can be derived from W as (Truesdell and Noll, 1965)

$$\sigma_{ij} = -p\delta_{ij} + 2\frac{\partial W}{\partial I_1}B_{ij} - 2\frac{\partial W}{\partial I_2}(B^{-1})_{ij}. \tag{54}$$

where p is the hydrostatic pressure.

The material constants C_{ij} in (53) are determined by fitting to the experimental data. Here, we consider a rubber with the material constants (Goldberg, 1976; Morman, 1981)

$$C_{10} = 1.008 \times 10^{-1}\ \text{MPa} \tag{55}$$

$$C_{01} = 1.612 \times 10^{-1}\ \text{MPa} \tag{56}$$

$$C_{11} = 1.338 \times 10^{-3}\ \text{MPa} \tag{57}$$

$$C_{20} = 6.206 \times 10^{-4}\ \text{MPa} \tag{58}$$

$$C_{30} = 6.206 \times 10^{-9}\ \text{MPa}. \tag{59}$$

We also consider a Mooney–Rivlin material with the constants (Oden, 1972)

$$C_{10} = 0.550\ \text{MPa} \tag{60}$$

$$C_{01} = 0.138\ \text{MPa} \tag{61}$$

$$C_{11} = C_{20} = C_{30} = 0. \tag{62}$$

In addition, we consider a neo-Hookean material with the constants

$$C_{10} = 0.5\ \text{MPa} \tag{63}$$

$$C_{01} = C_{11} = C_{20} = C_{30} = 0. \tag{64}$$

For the neo-Hookean material, the only nonzero constant C_{10} is related to the shear modulus of rubber, G, as $C_{10} = G/2$. The values of G for rubbers generally lie between 0.2 and 1.0 MPa.

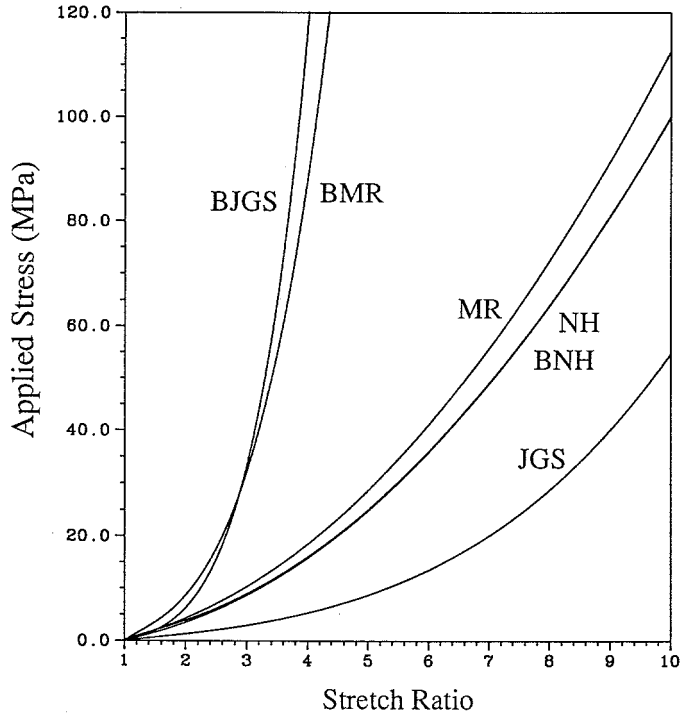

Figure 5. The stresses as functions of the stretch ratio for three nonlinearly elastic materials. Curves NH, MR, and JGS represent the NH, MR, and JGS rubbers under uniaxial tensile loading conditions, respectively. Curves BNH, BMR, and BJGS represent the NH, MR, JGS rubbers under equal biaxial tensile loading conditions, respectively.

In the following, we denote the material with the material constants in (55) to (59) as the JGS rubber. We denote the Mooney–Rivlin material with the material constants in (60) to (62) as the MR rubber. We denote the neo-Hookean material with the material constants in (63) and (64) as the NH rubber.

In Figure 5, the applied stresses as functions of the stretch ratio under uniaxial tensile loading and equal biaxial tensile loading for the JGS, MR, and NH rubbers are plotted. In the figure, the curves for the JGS, MR, and NH rubbers under uniaxial tensile loading are represented by JGS, MR, and NH, respectively. The curves for the JGS, MR, and NH rubbers under equal biaxial tensile loading are represented by BJGS, BMR, and BNH, respectively. Since the material elements on the void surface are subjected to equal biaxial loading conditions (due to spherical symmetry), curves BJGS, BMR, and BNH in Figure 5 represent the constitutive relations for these material elements and therefore have important implications on the modeling of void expansion in rubber particles. It should be noted that the neo-Hookean material (the NH rubber) has almost the same response at large strains under both uniaxial and biaxial tensile loading conditions, as shown by curves NH and BNH. The JGS and MR rubbers are very stiff under equal biaxial loading conditions. For example, curves BMR and BJGS in Figure 5 show that the stresses at the stretch ratio $\lambda = 4$ are about 80 MPa and 120 MPa, which are larger than the yield stresses of the typical plastic matrices in which the rubber particles are embedded for toughening. The stresses increase very sharply when the stretch ratio λ becomes larger than 4.

3.2. FORMULATION

Due to symmetry, the stretch ratio in the hoop direction, λ, can be simply represented as

$$\lambda = R/r, \tag{65}$$

where r and R represents the radial coordinate of a material point before and after deformation, respectively. Due to symmetry, the off-diagonal components of **B** are zero. The diagonal components of **B** are denoted as B_R, B_θ, and B_ϕ. We have

$$B_\theta = B_\phi = \lambda^2. \tag{66}$$

The incompressibility gives

$$I_3 = B_R B_\theta B_\phi = 1. \tag{67}$$

Then, B_R can be derived as

$$B_R = \lambda^{-4}. \tag{68}$$

Substituting (66) and (68) into (54) gives the relations between the stresses and the stretch ratio λ as in Chang and Pan (1998)

$$\begin{aligned}\sigma_R \;=\; & -p - 4C_{11}\lambda^6 + (-2C_{01} + 6C_{11})\lambda^4 + 24C_{30} + (-72C_{30} + 8C_{20})\lambda^{-2} \\ & +(-6C_{11} + 54C_{30} + 2C_{10} - 12C_{20})\lambda^{-4} + (4C_{11} + 24C_{30})\lambda^{-6} \\ & +(4C_{20} - 36C_{30})\lambda^{-8} + 6C_{30}\lambda^{-12}\end{aligned} \tag{69}$$

$$\begin{aligned}\sigma_\theta \;=\; & -p + (2C_{11} + 24C_{30})\lambda^6 + (-72C_{30} + 8C_{20})\lambda^4 \\ & +(-6C_{11} + 54C_{30} + 2C_{10} - 12C_{20})\lambda^2 + 24C_{30} \\ & +(4C_{20} - 36C_{30} - 2C_{01} + 6C_{11})\lambda^{-2} + (6C_{30} - 2C_{11})\lambda^{-6}\end{aligned} \tag{70}$$

$$\sigma_\phi = \sigma_\theta. \tag{71}$$

Here p is a function R. The off-diagonal stress components are equal to 0.

We now begin to solve the stress distribution within the rubber particle. The equilibrium equation is

$$\frac{\mathrm{d}\sigma_R}{\mathrm{d}R} + \frac{2}{R}(\sigma_R - \sigma_\theta) = 0. \tag{72}$$

The boundary conditions require

$$\sigma_R = 0 \quad \text{at} \quad R = R_b. \tag{73}$$

Substituting (69) and (70) into (72), we have

$$\begin{aligned}\frac{\mathrm{d}\sigma_R}{\mathrm{d}R} &= \frac{2}{R}\{(6C_{11}+24C_{30})\lambda^6+(-72C_{30}+8C_{20}+2C_{01}-6C_{11})\lambda^4\\ &\quad+(-6C_{11}+54C_{30}+2C_{10}-12C_{20})\lambda^2\\ &\quad+(-4C_{20}+36C_{30}-2C_{01}+6C_{11})\lambda^{-2}\\ &\quad+(6C_{11}-54C_{30}-2C_{10}+12C_{20})\lambda^{-4}+(-18C_{30}-6C_{11})\lambda^{-6}\\ &\quad+(-4C_{20}+36C_{30})\lambda^{-8}-6C_{30}\lambda^{-12}\}\end{aligned} \tag{74}$$

The volume conservation due to incompressibility gives

$$R^3-R_b^3=r^3-r_b^3. \tag{75}$$

Therefore, the stretch ratio λ in (74) can be expressed as

$$\lambda=\frac{R}{r}=\frac{R}{(R^3-R_b^3+r_b^3)^{1/3}}. \tag{76}$$

Substituting $R=R_0$ into (75) gives the expansion ratio of the outer radius of the rubber particle as

$$\frac{R_0}{r}=\left[1-\left(\frac{r_b}{r_0}\right)^3+\left(\frac{R_b}{r_0}\right)^3\right]^{\frac{1}{3}}. \tag{77}$$

Note that all the length scales are normalized by r_0 here. Also note that in (77), the initial radius of the void r_b/r_0 is given as an input for the problem and the final radius of the void R_b/r_0 can be obtained by solving the governing equations in the rubber particle and the plastic matrix.

Our numerical procedure to obtain the relation between the expansion ratio for the outer radius of the rubber particle R_0/r_0 and the remote radial stress σ_∞/σ_0 is explained in the following. The size of the plastic region C in the plastic matrix is first given as an initial guess. Then, the stresses σ_R and σ_θ, and the displacement u_R are integrated by the Runge–Kutta integration scheme from $R=C$ inward toward the outer radius of the rubber particle with use of the governing equations, (32), (30), and (31), and the boundary conditions, (20), (21), and (22). At $R=R_0$, the relation

$$\frac{R_0}{r_0}=1+\frac{u_r}{r_0} \tag{78}$$

must be satisfied.

During the Runge–Kutta integration for the stresses and displacement in the plastic matrix, (78) is checked at each increment of R. When the residual of (78) changes its sign, we can obtain the two values of R between which the solution of R_0 is located. The bisection iteration method is then applied to find the value of R_0 to satisfy (78). Once the value of R_0 is obtained for the assumed C, the conservation of the total volume of the rubber particle gives

$$\frac{R_b}{r_0}=\left[\left(\frac{R_0}{r_0}\right)^3+\left(\frac{r_b}{r_0}\right)^3-1\right]^{\frac{1}{3}}. \tag{79}$$

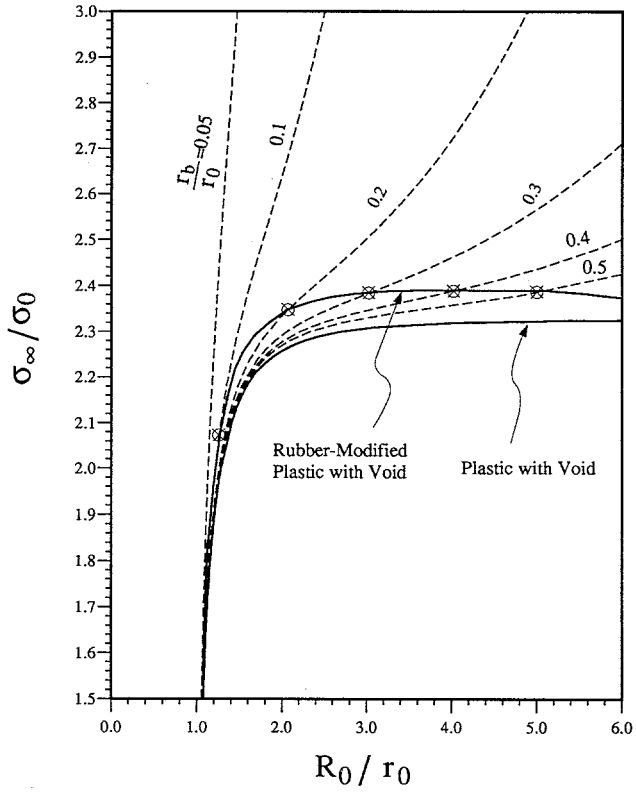

Figure 6. The normalized remote radial stresses σ_∞/σ_0 as functions of the expansion ratio of the rubber particle, R_0/r_0, for a void rubber-modified plastic. The material constants of the plastic matrix are $\sigma_0 = 75$ MPa, $\nu = 0.4$, $\sigma_0/E = 0.025$, $n = 10$, $\mu = 0.13$, and $\beta = 0$. The constitutive behavior of the rubber particle follows that of the JGS rubber. The two solid lines represents two bounds for the response of the rubber-modified plastic.

At $R = R_0$, we apply the continuity conditions of σ_R and u_R. Then, the stress σ_R is integrated from $R = R_0$ to $R = R_b$ with the use of (74). The traction-free boundary condition at $R = R_b$ cannot be satisfied unless the value of C is chosen correctly. Therefore, numerical iterations are performed to find the value of C to satisfy the traction-free condition

$$\sigma_R = 0 \quad \text{at} \quad R = R_b. \tag{80}$$

Note that σ_θ can be discontinuous at $R = R_0$ where the interface of the two materials is located.

3.3. Numerical results

The relations between the normalized remote radial stress σ_∞/σ_0 and the expansion ratio of the outer radius of the rubber particle R_0/r_0 are shown in Figure 6 for voided rubber-modified plastics. The material properties of the plastic matrix are $\nu = 0.4$, $n = 10$, $\mu = 0.13$, $\beta = 0$, and $\sigma_0 = 75$ MPa. These are typical material properties of epoxies used in Jeong and Pan, (1996). We first consider the JGS rubber with the constants described in (55) to (59) in this study. In Figure 6, the lower solid curve represents the relation between the normalized remote radial stress σ_∞/σ_0 and the void expansion ratio R_0/r_0 for the voided

plastic without the rubber particle. Also in Figure 6, the dashed curves represent the relations between the normalized remote radial stress σ_∞/σ_0 and the expansion ratio of the outer radius of the rubber particle R_0/r_0 in the rubber-modified plastic with different initial void sizes, $r_b/r_0 = 0.05, 0.1, 0.2, 0.3, 0.4$, and 0.5. As shown in Figure 6, as the initial void radius r_b/r_0 increases, the relation between σ_∞/σ_0 and R_0/r_0 for the rubber-modified plastic becomes closer to that of the voided plastic without the rubber particle. However, when the initial void radius r_b/r_0 in the rubber particle decreases, the rubber-modified plastic appears very stiff as σ_∞/σ_0 increases. The trend indicates that when the initial void size in the rubber particle becomes infinitesimal, no cavitation stress should be observed. This trend is similar to that shown in the pre-existing void model for the JGS rubber in Chang and Pan (1998).

Because a rubber material element cannot be extended to infinite stretch ratio, a failure mechanism at large strains should be considered. Note that the material elements on the void surface of the rubber particle are under plane stress, equal biaxial stretching conditions. For vulcanised rubber, the values of the critical stretch ratio at failure under biaxial stretching conditions are between 3.5 to 4 (Lazzeri and Bucknall, 1993). We adopt a simple failure criterion such that rupture occurs when the stretch ratio λ reaches 10 under plane-stress, equal biaxial loading conditions (Gent and Wang, 1991). If we select a smaller value of $\lambda = 4$ at failure, the results will not be shown clearly in our presentation. Therefore, when the stretch ratio λ of the material elements on the void surface of the rubber particle reaches 10, the rubber material elements are considered to fail. Then these material elements are no longer considered for carrying load and can be treated as being conceptually removed from our consideration. We assume that no permanent deformation occurs in the rubber before rupture and the deformation in the rubber is elastic and recoverable. Then the rubber material will adjust the deformation and stresses to those of a rubber-modified plastic with a smaller amount of initial rubber material (or a larger initial void size).

As we gradually increase the remote radial stress σ_∞/σ_0, an infinitesimal void starts to expand. When the material elements on the void surface reach the stretch ratio $\lambda = 10$, they fail. For a given value of r_b/r_0, we can find a remote radial stress σ_∞/σ_0 under which the stretch ratio λ for the material elements on the void surface is 10. The deformation and stress fields of the rubber-modified plastic with the ratio of r_b/r_0 at this σ_∞/σ_0 are basically the same as those of the rubber-modified plastic with an initially infinitesimal void but with some inner portion of the rubber particle being ruptured and conceptually removed. Based on this principle, a solid curve can be drawn in Figure 6 by connecting the point on each dashed line where the stretch ratio λ on the void surface is 10. This solid curve becomes the relation between R_0/r_0 and σ_∞/σ_0 for the rubber-modified plastic with an initially infinitesimal void in the rubber particle with consideration of rubber failure. As we can see in Figure 6, the maximum difference of the values of σ_∞/σ_0 for the voided plastic and the voided rubber-modified plastic is less than 5 percent at a given large R_0/r_0. This difference becomes even smaller if a smaller stretch ratio at failure is assumed.

It should be noted that other non-symmetric rupture mechanisms such as radial cracks can occur. When the cracks are initiated and grown, the load-carrying capacity of the rubber will further decrease. Here, the biaxial rupture stretch ratio is assumed to be relatively large (at 10) here. Therefore, the two solid curves in Figure 6 can be regarded as an upper bound and a lower bound for the rubber-modified plastic. At $R_0/r_0 = 10$, the rubber particle should fail completely under this condition and the upper and lower solid curves should merge together. If we select a smaller value of $\lambda = 4$ at failure, the upper solid curve will be very close to the lower solid curve. From this observation and a closer examination of the upper solid curve

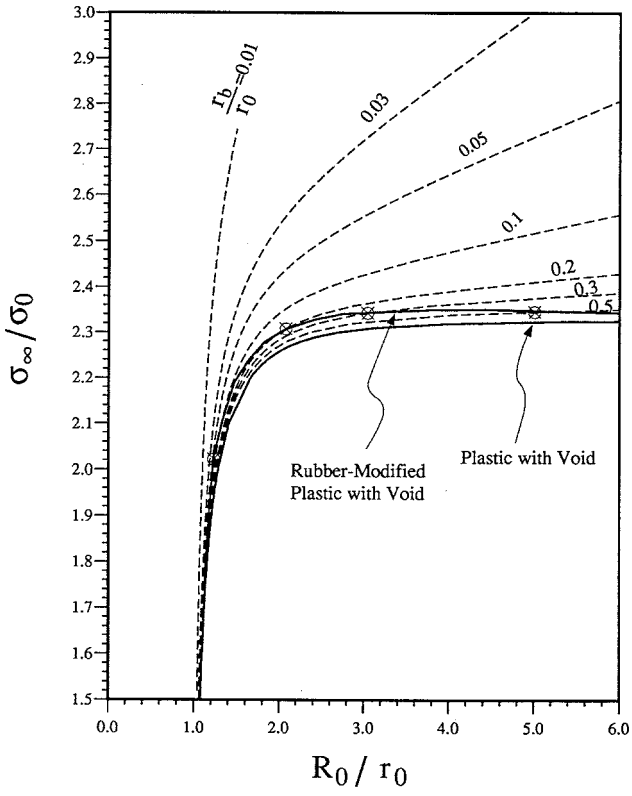

Figure 7. The normalized remote radial stresses σ_∞/σ_0 as functions of the expansion ratio of the rubber particle, R_0/r_0, for a voided rubber-modified plastic. The material constants of the plastic matrix are $\sigma_0 = 75$ MPa, $\nu = 0.4$, $\sigma_0/E = 0.025$, $n = 10$, $\mu = 0.13$, and $\beta = 0$. The constitutive behavior of the rubber particle follows that of the MR rubber. The two solid lines represents two bounds for the response of the rubber-modified plastic.

in Figure 6, we find that there is a maximum value of σ_∞/σ_0 between $R_0/R_b = 3$ and 5. When the rubber-modified plastic is subjected to load-controlled conditions, the maximum stress should be regarded as the cavitation instability stress when the strain failure criterion is employed.

Figure 7 shows the results for the plastic containing the Mooney–Rivlin rubber particle. The lower solid curve represents the relation between σ_∞/σ_0 and R_0/r_0 for the voided plastic without the rubber particle. When no failure criterion is considered for the rubber-modified plastic, the dashed lines shown in the figure indicate that there is no cavitation phenomenon as r_b/r_0 decreases. However, when a failure criterion at $\lambda = 10$ is considered under biaxial stretching conditions, the relation between σ_∞/σ_0 and R_0/r_0 for the rubber-modified plastic with an initially infinitesimal void in the rubber particle can be obtained and shown as the upper solid curve in Figure 7. The upper solid curve indicates that cavitation stress exists as in the plastic containing the JGS rubber as shown in Figure 6.

For the plastic containing the neo-Hookean rubber particle, when a failure criterion is not considered, the relation between σ_∞/σ_0 and R_0/r_0 is almost the same as that for the plastic itself. When a failure criterion is considered, the relation between σ_∞/σ_0 and R_0/r_0 becomes even closer to that for the plastic itself. Therefore the results will not be shown here.

Yee and Pearson (1986) and Pearson and Yee (1986) examined the fracture surface of single-edge notched three-point-bend specimens of rubber-modified epoxies. They showed that the diameter of the cavity formed from the rubber particle on the fracture surface can increase up to 200 percent when compared to the diameter of the rubber particle before deformation. This observation indicates that the plastic matrix itself fractures at finite strains or stresses. Mathematically, we can assume that the plastic matrix fractures when a critical stress or strain criterion is satisfied. We can apply the same principle for rubber rupture to the plastic. For example, we can assume that the plastic fractures at the stretch ratio of 2. This corresponds to the expansion ratio of $R_0/r_0 = 2$ for the voided plastic. For all the curves shown in Figures 2 and 3, the normalized remote radial stress σ_∞/σ_0 at $R_0/r_0 = 2$ is within 5 percent of the corresponding critical cavitation stress S/σ_0. Note again that when a strain failure criterion is considered for the rubber, the stress-expansion ratio relations and the cavitation stresses for the plastic with and without the rubber particle become very close to each other. Therefore the general trend of the critical cavitation stresses presented here should be very similar to the general trend of the stresses under which the plastic matrix starts to fracture at the critical expansion ratio $R_0/r_0 = 2$. Thus our results presented here should be useful to understand the fracture mechanisms in rubber-modified plastics.

4. Conclusion

In this paper, we have investigated the spherical void expansion in plastics and rubber-modified plastics under remote radial traction. First, the effects of pressure sensitivity on the cavitation stresses in plastics are examined. Our results show that, in general, the cavitation stress in plastics decreases as the pressure sensitivity increases and/or the plastic dilatancy factor decreases. For example, the normalized cavitation stress, S/σ_0, of plastics decreases by a factor of 1.75 when the pressure sensitivity μ increases from 0 to 0.3 with $\beta = 0$. The decrease of cavitation stress due to the pressure sensitivity and the large ratio of the yield stress to the modulus in plastics may imply the crack resistance curves may be relatively lower when compared to those of metals (Tvergaard and Hutchinson, 1992).

When the rubber particles in plastic is characterized by the neo-Hookean strain energy function, our results indicate that, with and without considering a failure criterion for rubber, the cavitation stress in the rubber-modified plastic is almost the same as that for the plastic. As shown from the trend in Figure 6 and 7, when there is a small void in the rubber particle, the rubber-modified plastic is very stiff and shows no cavitation phenomenon when the rubber is characterized by the Mooney–Rivlin strain energy function and the third-order strain energy function of James, Green and Simpson (1975). However, when a strain failure criterion is considered, the stress-expansion ratio relations and the cavitation stresses for the plastic with and without the rubber particle become very close to each other. The results suggest that the computational investigation of the crack-tip fields in rubber-modified epoxies in Jeong and Pan (1996) is reasonable by using a generalized Gurson's yield criterion for pressure-sensitive voided materials to represent the constitutive behavior of rubber-modified epoxies.

Appendix A: Closed-form solutions for incompressible materials

In this appendix, simple closed-form solutions for the normalized radial stress σ_∞/σ_0 as functions of the void expansion ration R_0/r_0 are obtained for two special cases: Mises materials with $\nu = 1/2$, and pressure-sensitive materials with $\beta = 0$ and $\nu = 1/2$. In these

two special cases, the governing equations for the displacement become simple due to the material incompressibility.

A.1. Elasticity incompressible Mises materials

For Mises materials, the governing equation of u_R is (50). When $\nu = \frac{1}{2}$, we have $F(R) = 0$ from (42). Therefore, (50) can be simplified to

$$\frac{\mathrm{d}u_R}{\mathrm{d}R} = 1 - \left(1 - \frac{u_R}{R}\right)^{-2}. \tag{A1}$$

The general solution of (A1) is

$$R^3 - (R - u_R)^3 = B, \tag{A2}$$

where B is a constant. Note that $r = R - u_R$. Substituting $R = R_0$ into (A2) gives

$$B = R_0^3 - r_0^3. \tag{A2}$$

Therefore, one can find that the governing equation of the displacement u_R, (A1), essentially satisfies

$$R^3 - R_0^3 = r^3 - r_0^3. \tag{A4}$$

Note that (A4) can be derived from the material incompressibility such that the total volume of the material between the void surface and the surface corresponding to a material point remains constant after deformation.

Substituting $R = C$ into (A4) gives

$$R_0^3 - r_0^3 = C^3 - (C - u_R^C)^3. \tag{A5}$$

Rearranging the above equation gives

$$\frac{R_0}{r_0} = \left\{1 - \left(\frac{C}{R_0}\right)^3 + \left(\frac{C}{R_0} - \frac{u_R^C}{R_0}\right)^3\right\}^{-\frac{1}{3}}. \tag{A6}$$

Substituting (48) and (49) into (A6) gives the void expansion ration R_0/r_0 in terms of the remote radial stress σ_∞/σ_0. After rearranging of the equation, we arrive at

$$\frac{\sigma_\infty}{\sigma_0} = \frac{2}{3}\left\{1 + \ln\left[1 - \left(\frac{R_0}{r_0}\right)^{-3}\right] - \ln\left[1 - \left(1 - \frac{\epsilon_0}{2}\right)^3\right]\right\}. \tag{A7}$$

where $\epsilon_0 = \sigma_0/E$. The critical cavitation stress S/σ_0 for Mises materials with $\nu = \frac{1}{2}$ is obtained when R_0/r_0 approaches to ∞ in (A7) as

$$\frac{S}{\sigma_0} = \frac{2}{3}\left\{1 - \ln\left[1 - \left(1 - \frac{\epsilon_0}{2}\right)^3\right]\right\}. \tag{A8}$$

When ϵ_0 is small, the first-order expansion of (A8) becomes

$$\frac{S}{\sigma_0} = \frac{2}{3}\left\{1 + \ln\left(\frac{2}{3\epsilon_0}\right)\right\}, \tag{A9}$$

which is the same as (2.10) in Huang et al. (1991).

A.2. Pressure-sensitive incompressible materials

For pressure-sensitive materials with $\beta = 0$ and $\nu = 1/2$, the governing equation of the displacement u_R, (44), can be reduced to the form in (A1). Therefore, the same simple relation for the displacement field in the inner plastic region can be represented by (A4), and also by (A6). Substituting (36), (37), (38) into (A6), a relation between the void expansion ratio and the normalized remote radial stress σ_∞/σ_0 can be obtained

$$\frac{R_0}{r_0} = \left\{1 - \left[\left(1 + \frac{2\mu}{\sqrt{3}}\right)\left(1 - \sqrt{3}\mu\frac{\sigma_\infty}{\sigma_0}\right)\right]^{-\sqrt{3}+2\mu/2\mu} \times \left\{1 - \left[1 - \frac{\epsilon_0}{2}\left(1 - \sqrt{3}\frac{\sigma_\infty}{\sigma_0}\right)\right]^3\right\}\right\}^{-\frac{1}{3}}. \tag{A10}$$

The critical cavitation stress S/σ_0 can be obtained from (A10) when R_0/r_0 approaches to ∞ as

$$\left[\left(1 + \frac{2\mu}{\sqrt{3}}\right)\left(1 - \sqrt{3}\mu\frac{S}{\sigma_0}\right)\right]^{-\sqrt{3}+2\mu/2\mu}\left\{1 - \left[1 - \frac{\epsilon_0}{2}\left(1 - \sqrt{3}\mu\frac{S}{\sigma_0}\right)\right]^3\right\} = 1. \tag{A11}$$

Therefore, S/σ_0 can be obtained by solving (A11). For small ϵ_0, (A11) can be approximated by

$$\left[\left(1 + \frac{2\mu}{\sqrt{3}}\right)\left(1 - \sqrt{3}\mu\frac{S}{\sigma_0}\right)\right]^{-\sqrt{3}+2\mu/2\mu}\left[\frac{3\epsilon_0}{2}\left(1 - \sqrt{3}\mu\frac{S}{\sigma_0}\right)\right] = 1. \tag{A12}$$

Solving (A12) for S/σ_0 gives

$$\frac{S}{\sigma_0} = \frac{1}{\sqrt{3}\mu}\left[1 - \left(\frac{2}{3\epsilon_0}\right)^{-2\mu/\sqrt{3}}\left(1 + \frac{2\mu}{\sqrt{3}}\right)^{-(1+2\mu/\sqrt{3})}\right]. \tag{A13}$$

Note that (A13) can be reduced to (A9) when $\mu \to 0$ by the L'Hôpital's rule.

Acknowledgement

The initial support of this work by the NSF under grant number DMR-8708405 is appreciated. Helpful discussion with Professor C.O. Horgan of University of Virginia is also appreciated.

References

Ashby, M.F., Blunt, F.J. and Bannister, M. (1989). Flow characteristics of highly constrained metal wires. *Acta Metallurgica* **37**, 1847–1857.

Ball, J.M. (1982). Discontinuous equilibrium solutions and cavitation in nonlinear elasticity. *Philosophical Transactions of the Royal Society of London* **A306**, 557–611.

Budiansky, B. (1959). A reassessment of deformation theories of plasticity. *Transactions of the American Society of Mechanical Engineers* **81E**, 259–264.

Chang, W.J. and Pan, J. (1998). Cavitation instability in rubber with consideration of failure submitted for publication in *Mathematics and Mechanics of Solids*.

Drucker, D.C. (1973). Plasticity theory, strength-differential (SD) phenomenon, and volume expansion in metals and plastics. *Metallurgical Transactions* **4**, 667–673.

Drucker, D.C. and Prager, W. (1952). Soil mechanics and plastic analysis or limit design. *Quarterly of Applied Mathematics* **10**, 157–165.

Gent, A.N. and Lindley, P.B. (1959). Internal rupture of bonded rubber cylinders in tension. *Proceedings of the Royal Society of London* **A249**, 195–205.

Gent, A.N. and Wang, C. (1991). Fracture mechanics and cavitation in rubber-like solids. *Journal of Materials Science* **26**, 339–3395.

Goldberg, W. (1967). An experimental investigation of non-linear isothermal viscoelasticity, Ph.D. Thesis, Purdue University.

Gurson, A.L. (1975). Plastic flow and fracture behavior of ductile materials incorporating void nucleation, growth and interaction. Ph.D. Thesis, Brown University.

Hill, R. (1950). *The Mathematical Theory of Plasticity*, Clarendon Press, Oxford.

Horgan, C.O. and Abeyaratne, R. (1986). A bifurcation problem for a compressible non-linearly elastic medium: growth of a micro-void. *Journal of Elasticity* **16**, 189–200.

Horgan, C.O. and Polignone, D.A. (1995). Cavitation in nonlinearly elastic solids: A review. *Applied Mechanics Reviews* **48**, 471–485.

Hou, H. and Abeyaratne, R. (1992). Cavitation in elastic and elastic-plastic solids. *Journal of the Mechanics and Physics of Solids* **40**, 571–592.

Huang, Y., Hutchinson, J.W. and Tvergaard, V. (1991). Cavitation instabilities in elastic-plastic solids. *Journal of the Mechanics and Physics of Solids* **39**, 223–241.

James, A.G. and Green, A. (1975). Strain energy functions of rubber. II. The characterization of filled vulcanizates. *Journal of Applied Polymer Science* **19**, 2319–2330.

James, A.G., Green, A. and Simpson, G.M. (1975). Strain energy functions of rubber. I. Characterization of gum vulcanizates. *Journal of Applied Polymer Science* **19**, 2033–2058.

Jeong, H.-Y. and Pan, J. (1996). Crack-tip fields for porous solids with pressure-sensitive matrices and for rubber-modified epoxies. *Polymer Engineering and Science* **36**, 2306–2319.

Lazzeri, A. and Bucknall, C.B. (1993). Dilatational bands in rubbber-toughened polymers. *Journal of Materials Science* **28**, 6799–6808.

Li, F.Z. and Pan, J. (1990a). Plane-strain crack-tip fields for pressure-sensitive dilatant materials. *Journal of Applied Mechanics* **57**, 40–49.

Li, F.Z. and Pan, J. (1990b). Plane-stress crack-tip fields for pressure-sensitive dilatant materials. *Engineering Fracture Mechanics* **35**, 1105–1116.

Morman, Jr. K.N., Kao, B.G. and Nagtegaal, J.C. (1981). Finite element analysis of viscoelastic elastomeric structures vibrating about non-linear statically stressed configurations. *Fourth International Conference of Vehicle Structural Mechanics*, Detroit, Michigan, 83–92.

Needleman, A. and Tvergaard, V. (1987). An analysis of ductile rupture modes at a crack tip. *Journal of the Mechanics and Physics of Solids* **35**, 151–183.

Oden, J.T. (1972). *Finite Element of Nonlinear Continua*, McGraw-Hill, New York.

Pearson, R.A. and Yee, A.F. (1986). Toughening mechanisms in elastomer-modified epoxies, Part 2. Microscopy studies. *Journal of Materials Science* **21**, 2457–2488.

Pearson, R.A. and Yee, A.F. (1991). Influence of particle size and particle size distribution on toughening mechanisms in rubber-modified epoxies. *Journal of Materials Science* **26**, 3828–3844.

Rice, J.R. and Tracey, D.M. (1969). On the ductile enlargement of voids in triaxial stress fields. *Journal of the Mechanics and Physics of Solids* **17**, 201–217.

Sue, H.-J. and Yee, A.F. Micromechanical modeling of crack-tip rubber particle cavitational process in polymer toughening. *Polymer Engineering and Science* **36**, 2320–2326.

Timoshenko, S.P. and Goodier, J.N. (1951). *Theory of ELasticity*, McGraw-Hill, New York.

Tvergaard, V. (1981). Influence of voids on shear band instabilities under plane strain conditions. *International Journal of Fracture* **17**, 389–407.

Tvergaard, V. (1982). On localization in ductile materials containing spherical voids. *International Journal of Fracture* **18**, 237–252.

Tvergaard, V. (1990). Material failure by void growth to coalescence. *Advances in Applied Mechanics* **27**, 83–151.

Tvergaard, V. and Hutchinson, J.W. (1992). The relation between crack growth resistance and fracture process parameters in elastic-plastic solids. *Journal of the Mechanics and Physics of Solids* **40**, 1377–1397.

Tvergaard, V., Huang, Y. and Hutchinson, J.W. (1992). Cavitation instabilities in a power hardening elastic-plastic solid. *European Journal of Mechanics, A/Solids* **11**, 215–231.

Truesdell, C. and Noll, W. (1965). The non-linear field theories of mechanics. *Encyclopedia of Physics III/3*. (Edited by S. Flugge), Springer-Verlag, Berlin.

Williams, M.L. and Schapery, R.A. (1965). Spherical flaw instability in hydrostatic tension. *International Journal of Fracture Mechanics* **1**, 64–71.

Xia, L. and Shih, C.F. (1995a). Ductile crack growth - I. A numerical study using computational cells with microstructurally-based length scales. *Journal of the Mechanics and Physics of SOlids* **43**, 233–259.

Xia, L. and Shih, C.F. (1995b). Ductile crack growth - II. void nucleation and geometry effects on macroscopic fracture behavior. *Journal of the Mechanics and Physics of Solids* **43**, 1953–1981.

Xia, L., Shih, C.F. and Hutchinson, J.W. (1995). A computational approach to ductile crack growth under large scale yielding conditions. *Journal of the Mechanics and Physics of Solids* **43**, 389–413.

Yee, A.F. and Pearson, R.A. (1986). Toughening mechanisms in elastomer-modified epoxies, Part 1. Mechanical studies. *Journals of Materials Science* **21**, 2462–2474.

Yee, A.F., Li, D. and Li, X. (1993). The importance of constraint relief caused by rubber cavitation in the toughening of epoxy. *Journal of Materials Science* **28**, 6392–6398.